Solar-Terrestrial Physics. 2025, vol. 11, iss. 3, pp. 59–69. DOI: 10.12737/stp-113202508. © 2025 A.V. Moiseev, V.I. Popov, V.V. Mishin, Yu.V. Penskikh. Published by INFRA-M Academic Publishing House

DOI: 10.12737/stp-113202508

Received March 08, 2025
Accepted May 22, 2025

FEATURES OF PROPAGATION OF COMPRESSIONAL LONG-PERIOD OSCILLATIONS PENETRATING FROM THE INTERPLANETARY MEDIUM IN THE MAGNETOSPHERE — IONOSPHERE SYSTEM

A.V. Moiseev
Yu.G. Shafer Institute of Cosmophysical Research and Aeronomy SB RAS, Yakutsk, Russia, moiseev@ikfia.ysn.ru

V.I. Popov
Yu.G. Shafer Institute of Cosmophysical Research and Aeronomy SB RAS, Yakutsk, Russia, volts@mail.ru

V.V. Mishin
Institute of Solar-Terrestrial Physics SB RAS, Irkutsk, Russia, vladm@iszf.irk.ru u

Yu.V. Penskikh
Institute of Solar-Terrestrial Physics SB RAS, Irkutsk, Russia, penskikh@iszf.irk.ru

Abstract. We have studied properties of Pi3 pulsations with a period of ~30 min in the magnetosphere—ionosphere system, using satellite and ground-based observations. According to the data from ground-based magnetic stations in the pre-noon sector of the magnetosphere, propagation of pulsations was revealed in azimuth from the dayside to the nightside at a velocity 3–9 km/s in the band of corrected geomagnetic latitudes Φ'=76°–79°. Along the meridian, the signal propagated poleward at a velocity 0.5–5 km/s. Analysis of signal spectra at stations located along different meridians shows three maxima: one latitude-independent maximum at a frequency of 0.55 mHz, and two latitude-dependent maxima at frequencies of 0.82 and 0.96 mHz respectively, at higher and lower latitudes. The first maximum corresponds to ULF waves penetrating from the solar wind; the other two, to magnetospheric field line resonances. The equivalent current system (ECS) during the pulsation recording was obtained by two methods: the method of spherical elementary current systems and the magnetogram inversion technique. Analysis of ECS derived by both methods has demonstrated that they match each other. The ECS during pulsations in the pre-noon sector is a large vortex consisting of smaller vortices that propagate in the ionosphere along the "sea-land" boundary line, i.e. meridional poleward propagation at velocities close to the average pulsation propagation velocities prevailed. According to the map of field-aligned current distribution in the ionosphere, the width of the maximum of the westward electrojet lies at the latitude of the ECS maximum (in the south of the large vortex) on the boundary between the regions of inflowing and outflowing field-aligned currents (regions 1 and 2), where field line resonances are observed. The obtained ECS corresponded to the DP2 current system with a predominant westward electrojet in the pre-noon and night sectors. Satellite data analysis has shown the following. In the solar wind, ULF waves in the Pi3 pulsation range propagated at a velocity of 186.4 km/s, which is significantly lower than the velocity of the medium being as high as 550 km/s. This velocity is explained by the fact that the waves propagate toward the Sun and are carried by the solar wind to Earth. In the magnetosphere, pulsations with a predominant compression component propagated from the nightside to the dayside at a velocity 90–110 km/s; from the delays in the onset of maxima of energetic electron differential fluxes, velocities 20–40 km/s were identified.

Pulsations in this event were caused by both external (oscillations in the solar wind) and internal sources (magnetospheric resonator, which could be excited, among other things, by a substorm). The dynamics of the "fine structure" of a large vortex — small vortices, in the magnetosphere as a whole coincides in propagation velocity and direction with geomagnetic pulsations.

Keywords: geomagnetic Pi3 pulsations, equivalent current vortices, azimuthal and meridional propagation, penetration of ULF waves from the interplanetary medium into the magnetosphere, field line resonance.

INTRODUCTION

It is known that Pi3 pulsations are irregular long-period oscillations in the geomagnetic field, which can be generated during a magnetospheric substorm [Saito, Matsushita, 1967]. The review [Saito, 1978] provides a classification according to which Pi3 is divided into subcategories: Ps6 and Pip. Ps6 pulsations (T>400–600 s) prevail in the D component of the geomagnetic field; Pip pulsations (T<400 s) have comparable amplitudes in all components. Sources of Pi3 and other geomagnetic pulsations are spatio-temporal variations in the intensity of three-dimensional current systems [Saito, 1969]. The Pi3 pulsations associated with a substorm are generally localized in the night sector of the magnetosphere. At the same time, the Pi3 pulsations are known to be linked with variations in interplanetary medium parameters

[Han et al., 2007]. Alimaganbetov and Streltsov [2018] have carried out a statistical analysis of wave disturbances in the solar wind (SW) during substorms and have found that wave disturbances with frequencies 0.6–0.7 mHz are often observed during substorms both in SW and on Earth. Presumably, Pi3s caused by outside forces should not only be recorded in the night sector of the magnetosphere, but also form a high-latitude current system of appropriate spatial scales.

It is known that the interaction of the diamagnetic structure (DS) with Earth's magnetosphere gives rise to phenomena similar to substorms, which can occur with Pi3 pulsations [Parkhomov et al., 2017]. These structures are in fact magnetic flux ropes filled with plasma [Eselevich, Eselevich, 2005]. A diamagnetic current flows on their surface, reducing the magnetic field inside and increasing it outside the flux tube.

An important characteristic of pulsations is their propagation whose direction may indicate their source. Moiseev et al. [2020] from ground-based geomagnetic observations have revealed azimuthal propagation of pulsations with a velocity 0.6–10.6 km/s to the east and west from midnight; along the meridian, the pulsations propagated to the equator at a velocity 0.75–7.87 km/s. Pulsation propagation can also be estimated from a shift of their current systems. In [Moiseev et al., 2024a], propagation velocities of geomagnetic pulsations localized on the dayside and designated as TCVs (traveling convection vortices) were compared with phase delays in the pulsations and based on motion of their equivalent current systems. The propagation velocities measured by these methods differ about two times (mostly in phase delays).

In this paper, we analyze the distribution of Pi3 pulsations recorded globally from ground-based and satellite observations. Field-aligned currents during pulsations are studied using the magnetogram inversion technique. As far as we know, the dynamics of global pulsations and vortices of the corresponding spatial scales have not been examined before.

The purpose of the work is to study the morphology and dynamics of large current vortices — a high-latitude current system of global Pi3 pulsations, as well as to assess the contribution of external and internal sources to the frequency spectrum of pulsations. For analysis, we have selected the September 11, 2015 event during which geomagnetic Pi3 pulsations were observed.

1. EXPERIMENTAL DATA

To examine meridional and azimuthal propagation of geomagnetic Pi3 pulsations and equivalent current vortices, we have used geomagnetic observations from the well-known SUPERMAG database [Gjerloev, 2012; https://supermag.jhuapl.edu/mag/]: coordinates of the stations are given in Tables 1 and 2. To construct equivalent current systems by the method of spherical elementary current systems (SECS), we have employed 61 SUPERMAG stations with geographic latitudes 45.14°–77.47° and longitudes 199.54°–267.89°; by the magnetogram inversion technique (MIT), 144 SUPERMAG stations in the Northern Hemisphere. Measurements from the CDAWEB database were used on satellites [http://cdawe b.gsfc.nasa.gov/]. Coordinates of the satellites are listed in Table 3. To study propagation, we rely on data from ground stations with a time resolution of 60 s since the duration of phase delays in signals ≥60 s. Satellite data had a time resolution of 3 (Themis), 60 (Geotail), 4 (Cluster), and 5 s (GOES).

2. ANALYSIS METHOD

We compared azimuthal propagation velocities obtained by two methods: from phase delays in magnetic variations at stations and from motion of vortices of equivalent ionospheric currents. The methods are described in [Moiseev et al., 2024b]. In the event of interest, there were pulsations with a well-defined shape at high latitudes, so their azimuthal propagation was studied only along corrected geomagnetic latitudes Φ'=76°–79°.

Field-aligned currents (FACs) of Pi3 pulsations were examined using MIT [Bazarzhapov et al., 1979; Mishin, 1990; Penskikh, 2020]. This method can calculate key electrodynamic parameters of the ionosphere with 1-min time resolution from data on the field of geomagnetic variations from the global network of ground magnetometers. In this work, with MIT we have obtained equivalent current functions, FACs with homogeneous conductivity, as well as boundaries of FAC zones [Lunyushkin, Penskikh, 2019; Penskikh et al., 2021]. To separate Pi3 pulsations from geomagnetic data, we employed a digital bandpass filter tuned to the frequencies corresponding to these pulsations [Moiseev et al., 2024b].

3. RESULTS

Figure 1 presents measurements of plasma and interplanetary magnetic field (IMF) parameters in SW: IMF components and ion concentration (*a*–*d*), V_x component of ion velocity and SW dynamic pressure P_d (*e*, *f*) from THEMIS-B (ThB) data in the September 11, 2015

Table 1

Coordinates of ground stations (SMAG) employed to study azimuthal propagation of pulsations

Average latitude	Abbreviation	Geographic coordinates		Corrected geomagnetic coordinates	
		latitude	longitude	latitude	longitude
76–79	GHC	68.63	264.15	77.54	–31.68
	IGC	69.30	278.2	78.43	–5.39
	UPN	72.78	303.85	78.93	40.20
	NAL	78.92	11.95	76.57	109.96
	DMH	76.77	341.37	77.34	84.38

Table 2

Coordinates of ground magnetometric stations,
used to study meridional propagation of geomagnetic pulsations

Abbreviation	Network	Geographic coordinates		Corrected geomagnetic coordinates	
		latitude	longitude	latitude	longitude
THL	GrW	77.47	290.77	84.72	29.24
SVS		76.02	294.9	83.00	32.87
KUV		74.57	302.82	80.69	41.92
UPN		72.78	303.85	78.93	40.20
UMQ		70.68	307.87	76.38	42.58
GDH		69.25	306.47	75.25	39.39
ATU		67.93	306.43	73.99	38.19
STF		67.02	309.28	72.64	40.87
SKT		65.42	307.10	71.43	37.22
FHB		62.00	310.32	67.41	39.05
NAQ		61.16	314.56	65.75	43.19
IGC	USAE	69.30	278.20	78.43	–5.39
RPB		66.52	273.77	75.99	–13.51
CDC		64.20	283.40	73.47	3.04
T47		62.20	284.35	71.51	4.23
T53		60.82	281.85	70.39	0.08
T46		60.05	282.71	69.60	1.36
T44		58.47	281.92	68.14	–0.04
T31		56.50	280.80	66.31	–1.92
T52		53.79	282.38	63.54	0.26
T51		48.05	282.22	57.86	–0.43
OTT		45.40	284.45	54.98	2.52
RES	USAC	74.69	265.11	82.93	–35.54
GHC		68.63	264.15	77.54	–31.68
BLC		64.32	263.99	73.60	–30.06
RAN		62.82	267.89	72.45	–23.12
FCC		58.76	265.91	68.50	–25.59
GIM		56.38	265.36	66.16	–26.08
PIN		50.20	263.96	59.96	–27.43
C08		45.87	264.92	55.72	–25.69
T56		45.59	267.03	55.60	–22.65
YKC	USAW	62.48	245.52	69.42	–56.85
SMI		60.03	248.07	67.48	–52.27
FMC		56.66	248.79	64.28	–50.02
T36		54.71	246.69	61.95	–52.09
C06		53.35	247.03	60.64	–51.24
RED		52.14	246.16	59.25	–51.96
T43		50.87	245.70	57.86	–52.17
T03		50.37	247.02	57.60	–50.40
LET		49.64	247.13	56.88	–50.07

event. At the bottom in panels *g*, *h* are the *AL* and *SYMH* indices for the interval considered. From 9:00 to 11:00 UT, three ~30 min oscillations were observed in IMF B_z and P_d, which manifested themselves on Earth's surface in *AL* variations and geomagnetic Pi3 pulsations. The oscillations were preceded by a period in which IMF B_z was southward from 07:30–09:00 UT. At that time, $B_x<0$, $B_y>0$, and the SW V_x component increased from 450 to 550 km/s. The ion concentration during this period varied in antiphase with IMF, such variations in plasma concentration and magnetic field are observed in DS [Parkhomov et al., 2017], and are also typical of slow mode oscillations [Hada, Kennel, 1985]. As the geomagnetic indices show, the event was recorded during a moderate magnetic storm and when an intense substorm, whose explosive phase lasted from 08:14 to 09:40 UT, ended.

Figure 2 illustrates changes in the magnetic field recorded by satellites in the noon and dawn sectors of the magnetosphere at 9:00–11:00 UT. Observations in SW are given with a shift of 10 min to make it easier to compare the shape of oscillations in SW and in the magnetosphere.

From top to bottom are B and $B_{x,y,z}$. Figure 3 displays the same data after bandpass filtering: the filter is seen to cause no phase distortions in raw signals. Variations in SW recorded by ThB, ThC and in the noon sector of the magnetosphere by Geotail (GL) are similar, which means that the pattern of field variations in the noon sector is largely due to their penetration from SW.

The ULF wave velocity V=186.4 km/s (lower than V_{SW}=550 km/s) was found from the phase delay in vari-

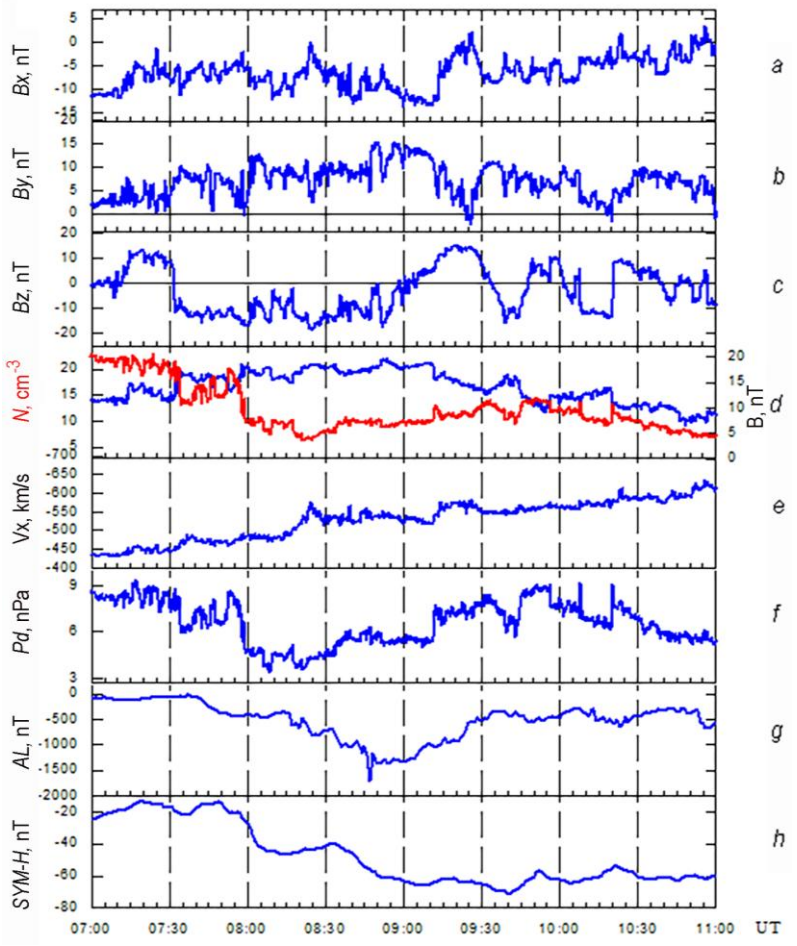

Figure 1. Plasma and interplanetary magnetic field parameters in SW: IMF component, its magnitude *B*, ion concentration (*a*–*d*), ion velocity V_x component, and SW dynamic pressure (*e*, *f*) according to THEMIS-B data in the September 11, 2015 event at 07:00–11:00 UT, *AL* and *SYMH* (*g*, *h*) for the period under study

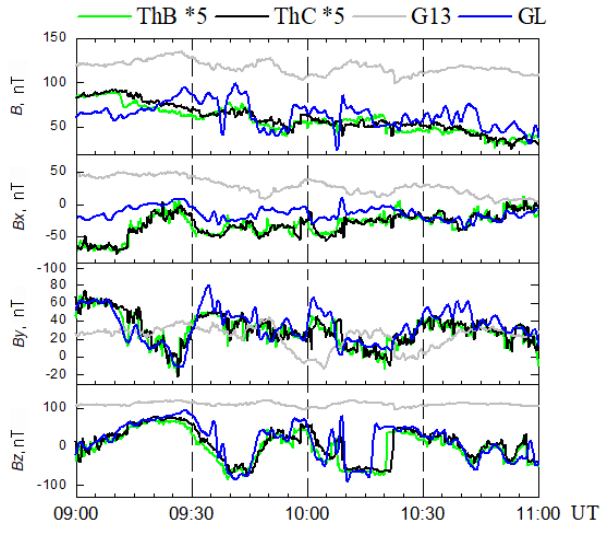

Figure 2. Satellite measurements of the magnetic field (*B* and $B_{x,y,z}$ in SW (THEMIS-B, THEMIS-C) and in the magnetosphere (GEOTAIL and GOES-13)). Data on SW is shifted by 10 min and is given with a weighted factor

ations of |**B**| between ThC and ThB and from the distance between them. We estimated the DS normal direction whose front was detected at 09:10 UT (see Figure 1). Parameters of the normal were calculated using the

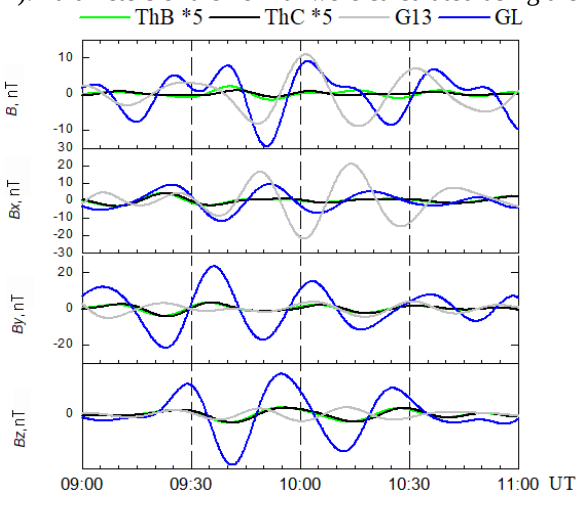

Figure 3. Satellite measurements of the magnetic field (*B* and $B_{x,y,z}$ in SW (THEMIS-B, THEMIS-C)) and in the magnetosphere (GEOTAIL and GOES-13) filtered within 1000–2400 s. Data on SW is shifted by 10 min and is given with a weighted factor

mixed data method [Abraham-Shrauner, Yun, 1976] and the complanarity theorem [Colburn, Sonett, 1966]

$$\mathbf{n} = \pm \frac{(\mathbf{B1}-\mathbf{B2})\times((\mathbf{B1}-\mathbf{B2})\times(\mathbf{V1}-\mathbf{V2}))}{\left|(\mathbf{B1}-\mathbf{B2})\times((\mathbf{B1}-\mathbf{B2})\times(\mathbf{V1}-\mathbf{V2}))\right|} \quad (1)$$

based on which the DS velocity was determined

$$\mathbf{V}_{DS}=((\rho 2\mathbf{V2}-\rho 1\mathbf{V1})\cdot\mathbf{n})/(\rho 2-\rho 1) \quad (2)$$

where **B**1, **V**1, ρ1, **B**2, **V**2, ρ2 are magnetic field, velocity, and plasma density ahead of and behind the DS front.

The normal to the DS front is directed toward the *Y* component (*n*=[0.095, 0.912, 0.3953] in the GSE coordinate system), the DS front velocity V_{DS}=182.8 km/s matches well the ULF wave propagation velocity in SW, determined above from phase delays between the satellites. The observed propagation velocities can be explained by the fact that ULF waves propagate upward along the incoming stream toward the Sun and are carried away by SW to Earth.

The field variations on GOES-13 (G13), located in the dawn sector, differ in frequency from those observed in the noon sector, and it is impossible to study propagation of pulsations from phase delays on these satellites.

Figure 4 exhibits the magnetic field magnitude *B*, the filtered magnetic field magnitude B_f, and the field-aligned component B_0 in Mean Field Aligned coordinates on satellites located in the sector from dawn to midnight local time. Measurements are shown from satellites located at 10:00 UT in the following MLT sectors: G13 (05 MLT), THEMIS-D (ThD, 04 MLT), GOES-15 (G15, 01 MLT), and CLUSTER-2 (C2, 02:30 MLT). The similarity in the waveform in the field magnitude on different satellites allows us to estimate the propagation velocity from the nightside to the dawnside: the velocity of C2-ThD is ~95 km/s; G15-G13, ~113.7 km/s. The similarity in the pulsation shape in the bottom and middle panels suggests a significant contribution of the SW compression component to geomagnetic pulsations, which is confirmed by B_0 whose maximum amplitude is observed in the noon sector; the minimum, in the midnight sector.

Table 3

Coordinates of satellites in the magnetosphere on September 11, 2015 at 10:00 UT in the GSE system

Satellites	GSE coordinates, R_e		
	X	Y	Z
THEMIS-B	61.78	–20.97	–3.26
THEMIS-C	60.27	–24.56	–3.94
GEOTAIL	8.59	3.62	–0.02
GOES-13	–1.64	–5.94	–2.39
THEMIS-D	–4.61	–9.03	–2.09
GOES-15	–6.35	–1.85	–0.19
CLUSTER-4	–8.70	–2.71	–12.05
CLUSTER-2	–10.07	–2.00	–11.39

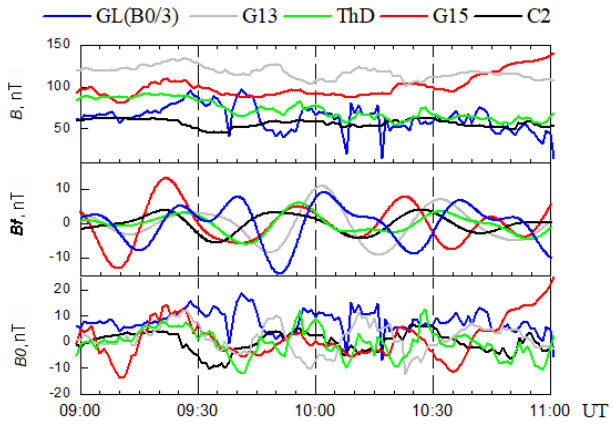

Figure 4. From top to bottom: the magnetic field magnitude *B*, the magnetic field magnitude B_f filtered within 1000–2400 s, the field-aligned component B_0 in Mean Field Aligned coordinates in the magnetosphere on GEOTAIL, GOES-13, THEMIS-D, GOES-15, and CLUSTER-2 satellites

Figure 5 illustrates the dynamics of energetic electron fluxes in the magnetosphere J_e=30–50 keV on G13 and G15, J_e=40 keV on ThD, and J_e>>40 keV on Cluster-4 (C4, 3 MLT). On satellites other than ThD, rapid increases in fluxes are seen to be replaced by slower decreases. This is due to the fact that particles gradually leave the localized region, where they were injected, through magnetic drift (on ThD, rates of increase and decrease in fluxes coincide). From phase delays in variations in the fluxes (indicated by arrows), we can conclude that J_e propagate from the nightside to the dayside at velocities of 39.3 (C4-ThD) and 23.8 km/s (ThD-G13). They are close to the propagation velocities of substorm injections (24 km/s) estimated in [Reeves et al., 1996].

Figure 6, *a* illustrates filtered variations in the *H* component of magnetometers distributed in azimuth at Φ′=76°–79°; on the right is the LT dependence of the azimuthal propagation velocity (*b*), FAC distributions constructed using MIT for a negative half-wave on magnetograms at 09:50–10:00 UT in panel *c*, for a positive half-wave at 10:05–10:20 UT (*d*); at the bottom are distributions of equivalent ionospheric currents constructed by the SECS method at the same time points (*e*, *f*). The dynamics of vortices was analyzed by this method based on a software code written in MatLab [Vanhamäki, Juusola, 2020], available at [https://link.springer.com/chapter/10.1007/ 978-3-030-26732-2_2#Sec18]. As follows from the phase delays in magnetic pulsations (panel *a*, the maxima from which propagation was analyzed are marked with asterisks),

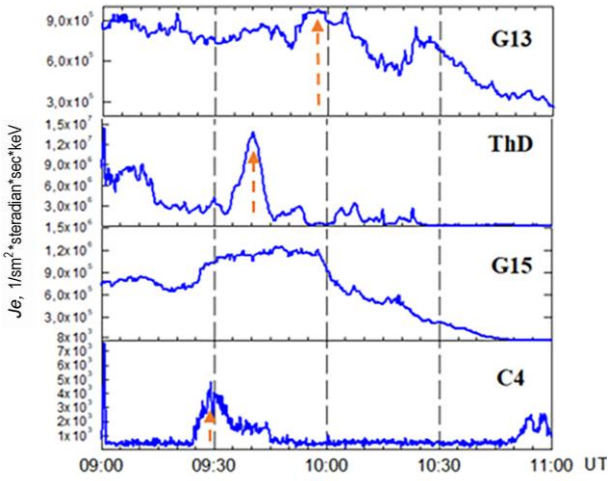

Figure 5. Fluxes of J_e=30–50 keV (GOES-13), 40 keV (THEMIS-D), 30–50 keV (GOES-15), J_e>40 keV (CLUSTER-4)

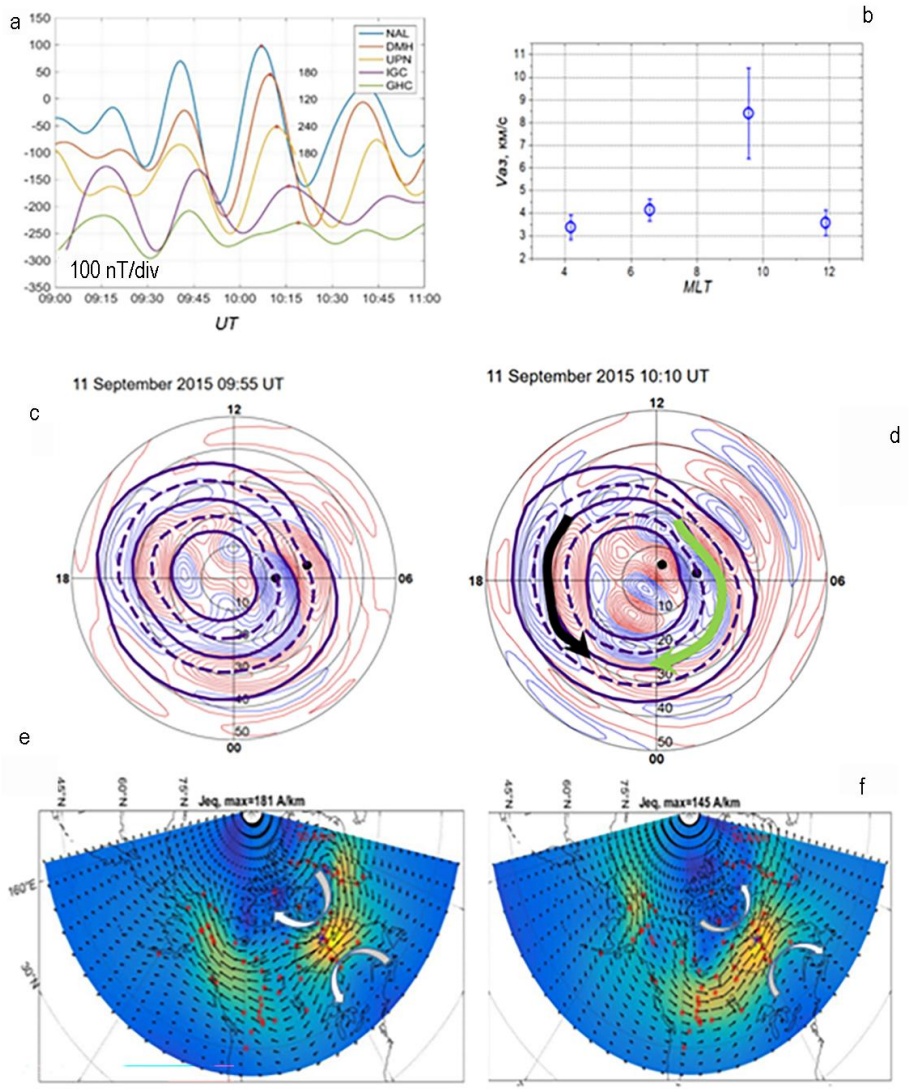

Figure 6. Geomagnetic field *H* component at azimuthally distributed stations at corrected geomagnetic latitudes 76°–79°, which was filtered within 1000–2400 s (*a*); MLT dependence of the azimuthal propagation velocity along Φ′=76°–79° (*b*); distribution of field-aligned currents with MIT (*c*, *d*); distribution of equivalent ionospheric currents with the SECS method (*e*, *f*) for a negative half-wave at 09:50–10:00 UT (*c*, *e*) and for a positive one at 10:05–10:20 UT (*d*, *f*) in geomagnetic Pi3 pulsations (panel *a*)

they propagated from the dayside to the nightside at velocities 3–9 km/s. The MIT FAC distribution maps show the inflowing (blue) and outflowing (red) FACs (panels *c*, *d*). Between sheets of opposite FACs, westward Hall currents are amplified in the dawn sector; and eastward ones, in the dusk sector (green and black arrows respectively in panel *d*). This location of the electrojets corresponds to the DP2 current system. The MIT FAC distribution maps indicate that during a positive half-wave the westward current is more extended in longitude and we can say that in addition to DP2 the DP1 current system is also amplified. SECS in panel *e* exhibits a large Hall vortex located in the dawn sector. The westward Hall current on the MIT maps corresponds to the lower part of this vortex at Φ′=70°–80°. According to the map of FAC distribution in the ionosphere, the latitudinal maximum of the westward electrojet is at the latitudes of maximum ECS (in the south of the large vortex) on the boundary between regions of inflowing and outflowing FACs (regions 1 and 2). For negative and positive half-waves, this current differs in direction due to the opposite directions of Hall currents inside and outside the vortex (the direction is indicated by white arrows in panels *e*, *f*). Oppositely directed ECSs were also recorded during global Pc5 pulsations [Huang, 2021].

We have analyzed the dynamics of the vortices indicated by white arrows (panel *f*): trajectories of the vortices, meridional and azimuthal propagation velocities are shown in Figure 7. Displacement trajectories of high-latitude (*a*) and low-latitude (*b*) vortices are located along the sea—land boundary line. The vortices propagate along the meridian to the north at velocities 1.6–4 km/s (*c*). Opposite propagation velocities ±25 km/s (*d*) are recorded along the azimuth, from which we can conclude that the vortices do not propagate along the azimuth. Localization of vortices along the sea—land boundary line can be attributed to the so-called coastal effects.

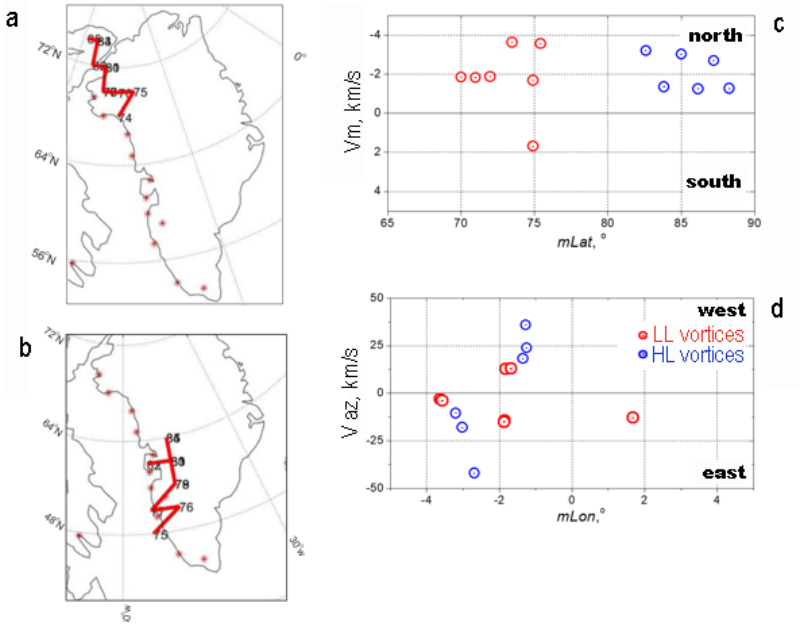

Figure 7. Vortex trajectories at higher (*a*) and lower (*b*) latitudes and velocities of meridional and azimuthal propagation along these trajectories (*c*, *d*) at 10:10–10:20 UT; LL, HL are low-latitude and high-latitude vortices

To study the frequency spectra of Pi3 pulsations, their dynamics in the meridional direction, as well as to identify latitudes of field line resonances, we have selected four meridional chains of ground magnetic stations whose coordinates are given in Table 2. Location of these chains is shown schematically in Figure 8, *c*. Panel *a* presents power spectra of ULF waves in SW, spectra of Pi3 pulsations on Earth at different latitudes, latitude dependence of the meridional velocity of pulsation propagation (*b*), and MLT dependence of westward electrojet and field line resonance latitudes (*d*). It can be seen (*a*) that the oscillation spectra in SW and on Earth have a common peak at a frequency of 0.55 mHz (designated by number 1), it shows up in all IMF components and in the SW velocity. Peaks at frequencies of 0.82 and 0.96 mHz (2.3) on spectrograms from ground stations have an explicit latitude dependence: they are observed with maximum intensity at higher and lower latitudes respectively. These peaks are also present in spectra of the interplanetary medium parameters B, B_z, and N. We determined the latitude of field line resonant oscillations Φ'_{FLR}, using the technique [Glassmeier et al., 1999], from maximum amplitude and phase difference of the oscillations along the meridional chain of stations. Φ'_{FLR} is plotted on distributions of meridional velocities of Pi3 pulsations along these meridians. It is apparent that poleward pulsation propagation along the meridian prevails to which correspond negative velocities 0.5–5 km/s; at Φ'_{FLR}, the velocities are subject to discontinuity. Locations of the westward electrojet and Φ'_{FLR} coincide (panel *d*).

4. DISCUSSION

Thus, we have studied the frequency spectrum and dynamics of global Pi3 pulsations at high latitudes and their equivalent current systems in the magnetosphere and ionosphere in the extended sector of longitudes 0–12 MLT. We have revealed that the pulsation spectrum has three peaks: at all latitudes at a frequency of 0.55 mHz, two peaks at 0.82 and 0.96 mHz at higher and lower latitudes respectively. We have found similar dynamics of small vortices, which are the fine structure of a large vortex, and pulsations in the ionosphere, but only along the meridian, as well as pulsation propagation from the dayside to the nightside in the ionosphere and in the opposite direction in the magnetosphere. The detected features are described below.

4.1. External and intramagnetospheric sources of Pi3 pulsations

In [Parkhomov et al., 1998], as in the event we deal with, two maxima were found in the spectrum of Pc5 pulsations: latitude-independent at 2.3 mHz and latitude-dependent at 4–6 mHz. The authors suggested that oscillations of the first type are associated with oscillations at the magnetopause, whereas oscillations of the second type are caused by intramagnetospheric resonances. The boundary of the FMS waveguide, the oscillations in which caused the first peak, according to their assumption, lies outside the magnetopause. In the event of interest, the latitude-independent peak of oscillations was detected at 0.55 mHz in SW, whereas ULF waves were recorded at 0.4–0.7 mHz. Latitude-dependent peaks at 0.82 and 0.96 mHz on ground-based magnetograms are present in IMF spectra and concentration. This is consistent with the conclusions drawn in [Kepko, Spence, 2003], in which when analyzing a number of geomagnetic pulsation events caused by P_d variations it has been found that discrete frequencies of intramagnetospheric resonances of 0.7, 1.3, 1.9, 2.6, and 3.4 mHz are observed in SW concentration variations and presumably reflect the existence of structures of certain sizes in the interplanetary medium. The oscillation frequencies in the event considered are close to the first harmonic of intramagnetospheric resonances, division by which is fair-

ly conventional.

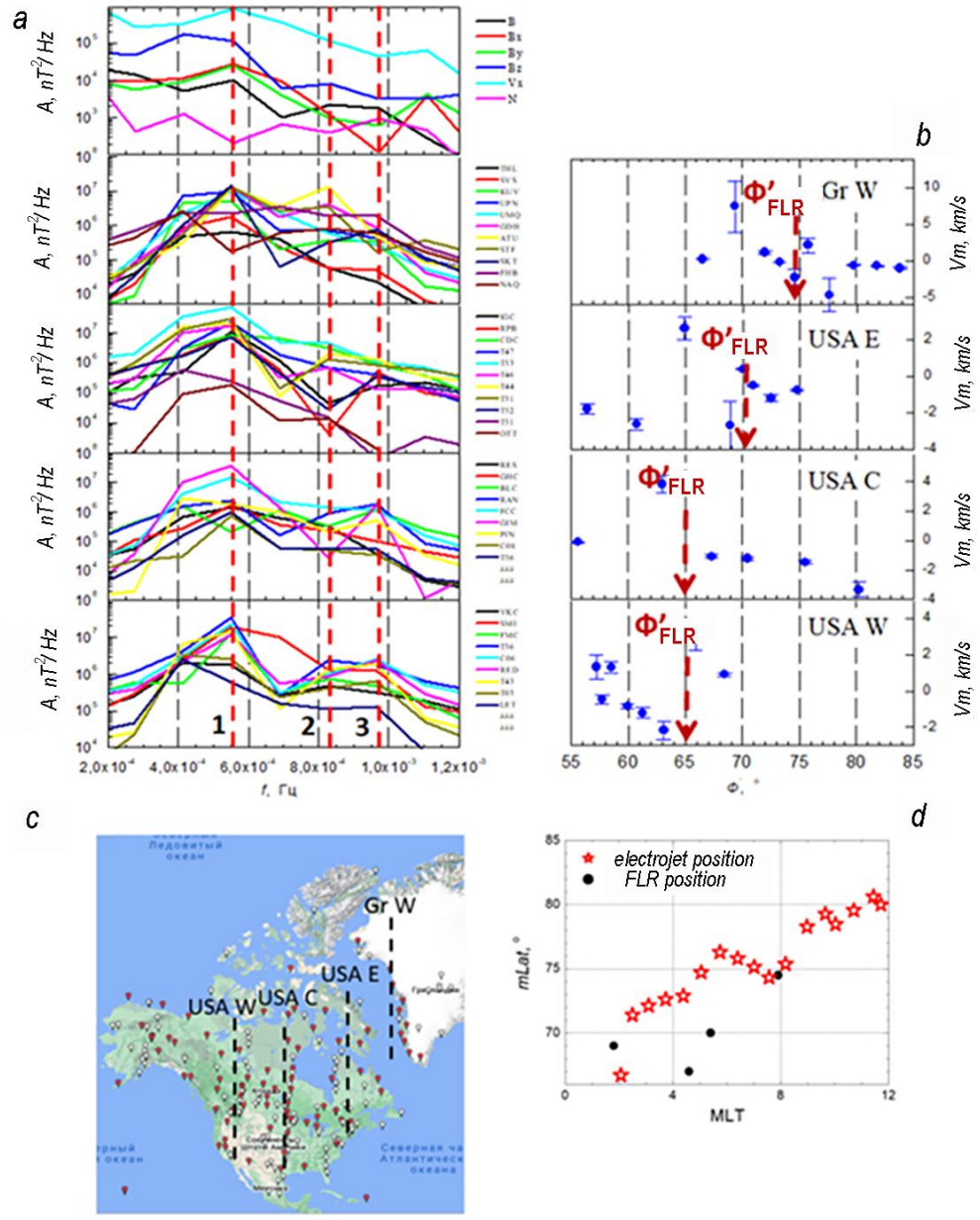

Figure 8. ULF wave spectra in SW, spectra of Pi3 pulsations on Earth at different latitudes, along different meridians (*a*), pulsation propagation velocities along different meridians (*b*), a map of meridional chains of stations (*c*), MLT dependence of the geomagnetic latitude of the westward electrojet and the latitude of field line resonances (*d*)

During the event of interest, several conditions are implemented which are favorable for penetration of waves from SW and for generation of globally recorded field variations in the magnetosphere: extreme IMF B_z, variations in P_d (ratio $\Delta P_d/P_d \sim 0.5$), and ~550 km/s SW velocity. Simultaneous variations in N and B are typical of compression MHD waves: fast magnetosonic (FMS) and slow magnetosonic (SMS). For an FMS wave, these parameters change in phase, and for an SMS wave they change in antiphase [Baumjohann and Treumann, 1996], which is observed in our case in the interplanetary medium and in the magnetosphere. The Alfvén SW velocity according to ThB data is ~90 km/s, which coincides by an order with the ULF wave velocity in SW (168 km/s); thus, waves in SW correspond to SMS waves. It should be added that Alfvén waves do not pass through the tangential discontinuity, which is the magnetopause, and MS waves can partially penetrate through it [Leonovich et al., 2003].

4.2. Dynamics of geomagnetic Pi3 pulsations and equivalent current vortices

Observations show that pulsations at latitudes Φ'=76°–79° propagate along the azimuth from the dayside to the nightside with V_{az}=3–9 km/s; along the meridian, poleward with V_m=0.5–5 km/s. The large Hall vortex ~3500 km in diameter, observed in the dawn sector, is generally stationary; however, there may be small vortices in it — the so-called fine structure of the large vortex 1000–1500 km in diameter. Small vortices also propagate poleward with comparable velocities 1.6–4 km/s.

Moiseev et al. [2024a, b] have examined meridional and azimuthal propagation of geomagnetic pulsations and 5–10 min small TCVs responsible for them. Comparison between propagation velocities of pulsations and vortices made in these works and in our work has shown that propagation velocities of pulsations and vortices coincide in the meridional direction, whereas in the azimuthal direction the vortices propagate faster with $V = 5$–25 km/s; in this case, TCVs do not experience a coastal effect and propagate along longitude in a sector up to 12 MLT. Both TCV and Pi3 phenomena are resonant, but if in the case of TCVs the location of their centers coincided with field line resonances (FLRs), in the case of Pi3 the location of FLR coincided with the westward electrojet, which is the lower part of the large vortex.

Huang [2021], when studying global Pc5 pulsations, has established that the pulsations did not propagate in the azimuthal direction; the author attributed the phase variation along the meridian to the evolution of the pulsation current system. The large vortex in the event considered does not propagate either, and to understand the difference in propagation of Pi3 pulsations and small vortices, we have examined azimuthal propagation at the same stations (see Figure 6, *a*) in terms of the *D* and *Z* components. Analysis of the components has revealed that no propagation was observed (not shown). Perhaps this explains the different dynamics of ECS and pulsations since all components are applied to ECS.

Coastal effects in auroras [Samsonov, Zaretsky, 1963; Nadubovich, 1967] and ionospheric currents [Shpynev et al., 1977] were actively studied from observations in the Soviet Arctic (a region in Yakutia with a center in Tixie Bay) during SibIZMIR and ICRA SB AS USSR expeditions in the winter of 1968–1969. These effects are naturally associated with the well-known Senko—Mansurov coastal effect [Senko, 1959; Mansurov, 1959], which implies that induced currents in the sea or land areas with increased conductivity are displaced to the shores or edges of these land areas due to the skin effect. Ionospheric effects involved an increase in the density of ionospheric currents in the coastline area, as well as the formation of regular vortex structures in ionospheric currents. Ionospheric projection of these phenomena was located on land at ~100–200 km from the boundary line. The SECS method allowed us to examine the evolution of small ionospheric vortices over time with 1-min resolution and to conclude that the location of the vortices at a distance of ~200 km from the coastline is consistent with the results obtained from the study of coastal ionospheric effects. Shpynev et al. [1977] state that local irregularities with spatial scales ~100–300 km are manifested in ionospheric coastal effects, which allows us to assume that small vortices 1000–1500 km in diameter (according to the SECS method) actually exist.

4.3. Comparison between satellite and ground-based measurements

Moiseev et al. [2020] have investigated the event of Pi3 pulsations whose sources were IMF B_z variations. In the magnetosphere in the range of Pi3 pulsations, propagation from the nightside to the dayside was found from phase delays in energetic electron fluxes and on Earth from phase delays in bay-like disturbances in riometric absorption. In this work, satellite and ground-based observations show the opposite propagation direction, and below we explore possible reasons for this.

To compare pulsation propagation observed on Earth and in the magnetosphere, ground stations located along latitudes $\Phi' = 76°$–$79°$ were projected into the equatorial plane of the magnetosphere by the Tsyganenko model Ts04 [Tsyganenko, Sitnov, 2005]. The projection of the ground stations and the location of the satellites in the equatorial plane of the magnetosphere on September 11, 2015 at 10:00 UT are shown in Figure 9. The minimum distance between field line projections corresponding to the ground stations and locations of the satellites are seen to be ~5 R_e. Thus, ground-based and satellite observations can cover different regions of the magnetosphere; therefore, the nature of pulsation propagation differs.

It is also possible that the propagation pattern we have recorded reflects the plasma convection direction: from the dayside to the nightside according to observations at high latitudes and in the opposite direction in the equatorial plane of the magnetosphere. This may be supported by the fact that the pulsation period of ~30 min makes it possible to classify them as Ps6 pulsations that are accompanied by auroras having a shape corresponding to the letter Ω [Akasofu, Kimball, 1964]. In the region of these auroras, convection is sunward in the equatorial plane and antisunward at high latitudes. Unfortunately, the lack of ground-based and satellite observations of auroras during this event does not allow us to draw definitive conclusions.

Using ThD observations, we have estimated the electric drift velocity (convection velocity) at 75 km/s, comparable to propagation velocities estimated from phase delays in both the magnetic field and energetic electron fluxes.

Using the Ts04 model, distances in the XY plane were estimated between projections of stations in the equatorial plane of the magnetosphere; and propagation velocities

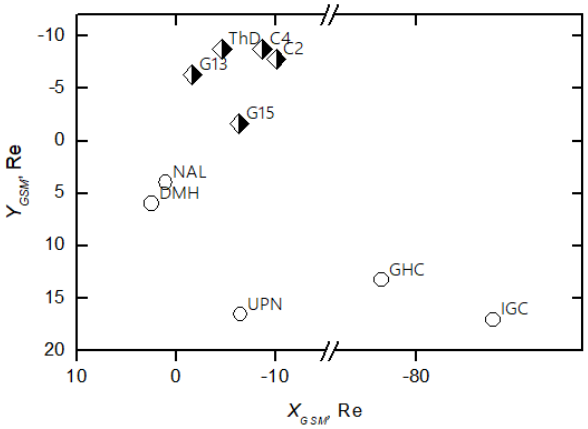

Figure 9. Projection of ground stations located along corrected geomagnetic latitudes 76°–79° (circles) and location of satellites (rhombs) in the equatorial plane of the magnetosphere on September 11, 2015 at 10:00 UT

V_{NAL_DMH}=86, V_{DMH_UPN}=734.2, V_{UPN_IGC}=2074.7, V_{IGC_GHC}=272.9 km/s, from ground-based time delays; the indices indicate the stations between which the velocities were measured. The minimum value of these velocities is in the order of the convection velocity, and the maximum value is close to the Alfvén velocity of 2225 km/s according to ThD data.

CONCLUSION

From the analysis we can draw the following conclusions. Propagation of Pi3 pulsations and small vortices coincides in magnitude and direction along the meridian. In the azimuthal direction, the vortices show the presence of a coastal effect. Propagation as observed on satellites and on Earth has the same direction as plasma convection: from the dayside to the nightside according to observations at high latitudes and in the opposite direction in the equatorial plane of the magnetosphere. ULF waves penetrating from SW and magnetospheric resonances also contribute to the frequency spectrum of pulsations.

Thus, we can conclude that pulsations in this event were caused by both external (oscillations in SW) and internal sources (the magnetospheric resonator that might have been excited by a substorm). The dynamics of the fine structure of a large vortex (small vortices) in the magnetosphere generally coincides in propagation velocity and direction with geomagnetic pulsations.

We are grateful to managers of the following projects for providing access to the data: SUPERMAG including the IMAGE network, (PI Liisa Juusola), GREENLAND COAST CHAIN data, (PI Anna N. Willer), Themis, CANMOS, Geomagnetism Unit of the Geological Survey of Canada; GIMA; Intermagnet; USGS, as well as satellite observation dataset from CDAWEB (D.J. McComas, R. Lepping, K. Ogilvi, G. Paschmann).

The results were obtained using data from the magnetometric complex included in the Shared Equipment Center «Angara» [http://ckp-angara.iszf.irk.ru/]. The work was carried out as part of the Government assignment (SHICRA SB RAS and ISTP SB RAS).

REFERENCES

Abraham-Shrauner B., Yun S.H. Interplanetary shocks seen by AMES plasma probe on Pioneer 6 and 7. *J. Geophys. Res*. 1976, vol. 81, pp. 2097–2102.

Akasofu S.I., Kimball D.S. The dynamics of the aurora: I. Instabilities of the aurora. *J. Atmos Terr. Phys.* 1964, vol. 26, pp. 205–211.

Alimaganbetov M., Streltsov A.V. ULF waves observed during substorms in the solar wind and on the ground. *J. Atmos. Solar-Terr. Phys*. 2018, vol. 181, pp. 10–18.

Baumjohann W., Treumann R.A. *Basic Space Plasma Physics*. Imperial College Press, London, 1996.

Bazarzhapov A.D., Matveev M.I., Mishin V.M. Geomagnetic variations and storms. Novosibirsk: Nauka, 1979, 248 p. (In Russian).

Colburn D.S., Sonett C.P. Discontinuities in the solar wind. *Space Sci. Rev*. 1966, vol. 5, pp. 439–506. DOI: 10.1007/BF0024 0575.

Eselevich M.V., Eselevich V.G. Fractal structure of the heliospheric plasma sheet in the Earth's orbit. *Geomagnetism and Aeronomy*. 2005, vol. 45, no. 3, pp. 326–336.

Gjerloev J.W. The SuperMAG data processing technique. *J. Geophys. Res.* 2012, vol. 117, no. A09213. DOI: 10.1029/ 2012JA017683.

Glassmeier K.-H., Othmer C., Gramm R., Stellmacher M., Engebretson M. Magnetospheric field-line resonances: A comparative planetology approach. *Earth Environment Sci*. 1999, vol. 20, pp. 61–109.

Hada T., Kennel C.F. Nonlinear evolution of slow waves in the solar wind. *J. Geophys. Res*. 1985, vol. 90, p. 531.

Han D.-S., Yang H.-G., Chen Z.-T., et al. Coupling of perturbations in the solar wind density to global Pi3 pulsations: A case study. *J. Geophys. Res.* 2007, vol. 112, A05217. DOI: 10.1029/2006JA011675.

Huang C.-S. Global Pc5 pulsations from the polar cap to the equator: Wave characteristics, phase variations, disturbance current system, and signal transmission. *J. Geophys. Res.* 2021, vol. 126, e2020JA029093. DOI: 10.1029/2020JA029093.

Kepko L., Spence H.E. Observations of discrete, global magnetospheric oscillations directly driven by solar wind density variations. *J. Geophys. Res*. 2003, vol. 108, p. 1257. DOI: 10.1029/2002JA009676.

Leonovich A.S., Mishin V.V., Cao J.B. Penetration of magnetosonic waves into the magnetosphere: Influence of a transition layer. *Ann. Geophys*. 2003, vol. 21, pp. 1083–1093.

Lunyushkin S.B., Penskikh Y.V. Diagnostics of auroral oval boundaries on the basis of the magnetogram inversion technique. *Sol.-Terr. Phys.* 2019, vol. 5, no. 2, pp. 97–113. DOI: 10.12737/stp-52201913.

Mansurov S.M. *Magnetic disturbances*. Moscow: Publ. House of the USSR Academy of Sciences, 1959, no. 1, pp. 64–71. (In Russian).

Mishin V.M. The magnetogram inversion technique and some applications. *Space Sci. Rev*. 1990, vol. 53, no. 1-2, pp. 83–163. DOI: 10.1007/bf00217429.

Moiseev A.V., Starodubtsev S.A., Mishin V.V. Features of excitation and azimuthal and meridional propagation of long-period Pi3 oscillations of the geomagnetic field on December 8, 2017. *Sol.-Terr. Phys*. 2020, vol. 6, no. 3, pp. 56–72. DOI: 10.12737/stp-63202007.

Moiseev A.V., Popov V.I., Starodubtsev S.A. Comparative analysis of the propagation of magnetic variations and equivalent current vortices of geomagnetic Pc5 pulsations along the meridian and azimuth. *Geomagnetism and Aeronomy*. 2024a, vol. 64, no. 4, pp. 548–566. DOI: 10.31857/ S0016794024040093.

Moiseev A.V., Popov V.I., Starodubtsev S.A. Investigating azimuthal propagation of Pc5 geomagnetic pulsations and their equivalent current vortices from ground-based and satellite data. *Sol.-Terr. Phys.* 2024b, vol. 10, no. 3, pp. 104–115. DOI: 10.12737/stp-103202412.

Nadubovich Yu.A. Collection of articles. Results of research on international geophysical projects. Polar aurora. Moscow: Nauka, 1967, no. 14, p. 77.

Parkhomov V.A., Mishin V.V., Borovik L.V. Long-period geomagnetic pulsations caused by the solar wind negative pressure impulse on March 22, 1979 (CDAW-6). *Ann. Geophys*. 1998, vol. 16, pp. 134–139.

Parhomov V.A., Borodkova N.L., Eselevich V.G., Eselevich M.V., Dmitriev A.V., Chilikin V.E. Features of the impact of the solar wind diamagnetic structure on Earth's magnetosphere. *Sol.-Terr. Phys.* 2017, vol. 3, no. 4, pp. 47–62. DOI: 10.12737/stp-34201705.

Penskikh Yu.V. Applying the method of maximum contributions to the magnetogram inversion technique. *Sol.-Terr. Phys.* 2020, vol. 6, no. 4, pp. 67–76. DOI: 10.12737/stp-64202009.

Penskikh Yu.V., Lunushkin S.B., Kapustin V.E. Geomagnetic method for automatic diagnostics of auroral oval boundaries in two hemispheres of Earth. *Sol.-Terr. Phys.* 2021, vol. 7, no. 2, pp. 57–69. DOI: 10.12737/stp-72202106.

Reeves G.D., Henderson M.G., McLachlan P.S., Belian R.D., Friedel R.H.W., Korth A. Radial propagation of substorm injections. *Proc. the Third International Conference on Substorms*. Eur. Space Agency Spec. Publ. 1996, ESA SP-389. p. 579.

Saito T. Geomagnetic pulsations. *Space Sci. Rev*. 1969, vol. 10, iss. 3, pp. 319–412.

Saito T. Long-period irregular magnetic pulsation Pi3. *Space Sci. Rev.* 1978, vol. 21, pp. 427–467. DOI: 10.1007/BF00173068.

Saito T., Matsushita S. Geomagnetic pulsations associated with sudden commencements and sudden impulses. *Planetary Space Sci*. 1967, vol. 15, pp. 573–587.

Samsonov V.P., Zaretsky N.S. Azimuthal and geographical distribution of auroral rays. *Geomagnetism and Aeronomy*. 1963, vol. 3, no. 2, p. 246.

Senko P.K. *Coastal effect in magnetic variations*. M.: 1959, 61 p.

Shpynev G.B., Mishin V.M., Mishin E.V. Research on geomagnetism, aeronomy and physics of the Sun. M.: Nauka, 1977, vol. 43, pp. 3–13.

Tsyganenko N.A., Sitnov M.I. Modeling the dynamics of the inner magnetosphere during strong geomagnetic storms. *J. Geophys. Res*. 2005, vol. 110, A03208. DOI: 10.1029/ 2004JA010798.

Vanhamäki H., Juusola L. Introduction to spherical elementary current systems. *Ionospheric Multi-Spacecraft Analysis Tools*. 2020, vol. 17, pp. 5–33. DOI: 10.1007/978-3-030-26732-2_13.

URL: https://supermag.jhuapl.edu/mag/ (accessed March 7, 2024).

URL: http://cdaweb.gsfc.nasa.gov/ (accessed March 7, 2024).

URL: https://link.springer.com/chapter/10.1007/978-3-030-26732-2_2#Sec18 (accessed March 7, 2024).

The paper is based on material presented at the 20th Annual Conference on Plasma Physics in the Solar System, February 10–14, 2025, Space Research Institute of the Russian Academy of Sciences, Moscow, Russia.

Original Russian version: Moiseev A.V., Popov V.I., Mishin V.V., Penskikh Yu.V., published in Solnechno-zemnaya fizika. 2025, vol. 11, no. 3, pp. 65–76. DOI: 10.12737/szf-113202508.

How to cite this article

Moiseev A.V., Popov V.I., Mishin V.V., Penskikh Yu.V. Features of propagation of compressional long-period oscillations penetrating from the interplanetary medium in the magnetosphere — ionosphere system. *Sol.-Terr.Phys.* 2025, vol. 11, iss. 3, pp. 59–69. DOI: 10.12737/stp-113202508.